Axon position within the corpus callosum determines contralateral cortical projection

Jing Zhou[a,b], Yunqing Wen[a], Liang She[a,b], Ya-nan Sui[a], Lu Liu[a,b], Linda J. Richards[c,d], and Mu-ming Poo[a,e,1]

[a]Institute of Neuroscience, State Key Laboratory of Neuroscience, Shanghai Institutes for Biological Sciences, Chinese Academy of Sciences, Shanghai 200031, China; [b]University of Chinese Academy of Sciences, Shanghai 200031, China; [c]Queensland Brain Institute and [d]School of Biomedical Sciences, the University of Queensland, Brisbane, Queensland, 4072, Australia; and [e]Department of Molecular and Cell Biology, Helen Wills Neuroscience Institute, University of California, Berkeley, CA 94720

Contributed by Mu-ming Poo, May 30, 2013 (sent for review May 1, 2013)

How developing axons in the corpus callosum (CC) achieve their homotopic projection to the contralateral cortex remains unclear. We found that axonal position within the CC plays a critical role in this projection. Labeling of nearby callosal axons in mice showed that callosal axons were segregated in an orderly fashion, with those from more medial cerebral cortex located more dorsally and subsequently projecting to more medial contralateral cortical regions. The normal axonal order within the CC was grossly disturbed when semaphorin3A/neuropilin-1 signaling was disrupted. However, the order in which axons were positioned within the CC still determined their contralateral projection, causing a severe disruption of the homotopic contralateral projection that persisted at postnatal day 30, when the normal developmental refinement of contralateral projections is completed in wild-type (WT) mice. Thus, the orderly positioning of axons within the CC is a primary determinant of how homotopic interhemispheric projections form in the contralateral cortex.

axon development | axon fiber order | cortical axon guidance | cortical development

The largest commissural tract in the human brain is the corpus callosum (CC), with more than 200 million axons connecting the two cerebral hemispheres. Callosal axons originate primarily from neurons of layer II/III and layer V of the neocortex (1) and project homotopically to the contralateral cortex. For example, callosal axons of the primary motor cortex (M1) and primary somatosensory cortex (S1) project to topographically equivalent locations in the contralateral M1 and S1, respectively. This pattern of homotopic projection is essential for coordinated motor and somatosensory functions as well as for higher associative and cognitive processes (2–4). Abnormal CC development has been noted in psychiatric and developmental disorders (5, 6), and deviant asymmetry of cortical areas found in patients with developmental dyslexia also may be attributed to callosal abnormalities (7, 8). However, the mechanism by which normal homotopic projection pattern is achieved during development remains largely unknown.

The majority of axonal projections in the nervous system are organized topographically. To facilitate the formation of orderly projections over long distances, axons originating from adjacent areas may preserve their topographic order within the nerve tract along their entire path toward the target region (9, 10). This preservation of topographic order has been shown in the thalamocortical tract (11–14) and in the optic and olfactory nerves (15–17). By performing a series of random microinjections of biotinylated dextran amine in the dorsal thalamus and reconstructing the labeled fibers, Powell et al. (14) showed that labeled axons within the thalamocortical tract preserve a topography similar to that in the ventral telencephalon before they reach the cortex. In the developing olfactory system, axons within the olfactory nerve from three different regions of the olfactory epithelia also are topographically segregated (17). Furthermore, signaling elicited by the axon guidance cue semaphorin3A (Sema3A) is required for such axon segregation within the olfactory nerve (17). Interestingly, previous immunostaining studies have shown that neuropilin-1 (Nrp1), a surface receptor for Sema3A, is expressed in the dorsal region of the CC in both human and mouse (18, 19), whereas the receptors for another axon guidance cue, ephrinA5, are restricted to the ventral CC (20, 21). These findings prompted us to inquire whether axons also are topographically segregated in an orderly manner within the CC and, if so, whether axonal position in the CC plays a role in the formation of homotopic axonal projections to the contralateral cortex after CC axons cross the midline.

To examine axonal order within the CC, we selectively labeled callosal axons from two adjacent cortical regions in the developing mouse cortex and traced their topography within the CC postnatally. Sequential in utero electroporation of vectors expressing EGFP and the red fluorescent protein mCherry in embryonic day 15.5 (E15.5) embryos allowed us simultaneously to label CC axons from two adjacent regions in one hemisphere. At postnatal day 8 (P8), we found that axons from these two cortical regions remained segregated in a specific order according to their anatomical origin within the CC, with axons from more medial regions located more dorsally within the CC. Furthermore, after midline crossing, dorsally located axons projected more medially in the contralateral cortex. When the expression of Sema3A or Nrp1 was manipulated, normal axon order within the CC was grossly disrupted, suggesting that Sema3A/Nrp1 signaling is responsible for regulating axon order within the CC. This role is consistent with the expression pattern of Sema3A and Nrp1 within and surrounding the CC. Interestingly, when axon order was grossly disrupted, we found that the projection of these axons still was determined by the axon position within the CC, thus resulting in a large number of abnormal heterotopic contralateral projections. In WT mice, minor aberrant heterotopic projections of M1 and S1 axons (22–24) observed at P8 were largely pruned by P30. However, gross heterotopic projections remained present in condi-

Significance

Two hemispheres of the neocortex are connected via a large axon bundle, the corpus callosum (CC). Axons from one side of the cortex project primarily to the equivalent cortical area on the contralateral side. How this homotopic axon projection is achieved during development remains unclear. Quantitative analysis of the cortical axons' positions within CC and their projection pattern after crossing the midline showed that axon position within CC is critical for homotopic projection. Further genetic perturbations of semaphorin/neuropilin-1 signaling disrupted the axon order in CC, resulting in an ectopic contralateral axon projection that could not be corrected by developmental refinement.

Author contributions: J.Z., L.J.R., and M.-m.P. designed research; J.Z. performed research; J.Z., Y.W., L.S., Y.-n.S., and L.L. analyzed data; and J.Z., L.J.R., and M.-m.P. wrote the paper.

The authors declare no conflict of interest.

[1]To whom correspondence should be addressed. E-mail: mpoo@berkeley.edu.

This article contains supporting information online at www.pnas.org/lookup/suppl/doi:10.1073/pnas.1310233110/-/DCSupplemental.

tional Nrp1-deletion mice at P30. Thus, Sema3A/Nrp1 signaling is essential for the order of axon positioning within the CC, and the axon's position within the callosal tract, regardless of its cortical origin, is the primary factor determining its initial contralateral projection.

Results

Axons from Different Cortical Regions Are Segregated in the CC. We first expressed EGFP and mCherry in layer II/III neurons of M1 and S1, respectively, by sequential in utero electroporation of vectors expressing these fluorescent proteins in E15.5 embryos (*Material and Methods*). Electroporated mouse brains were sectioned coronally (200 μm) at P8 and were examined for the distribution of labeled axons within the CC and for their targeting of contralateral cortices. Consistent with previous reports (6, 25, 26), we found that labeled M1 and S1 axons projected to corresponding contralateral M1 and S1 regions in the P8 mice (Fig. 1*A*). Moreover, using large-scale high-resolution confocal imaging at four different locations before and after midline crossing, we found that labeled M1 and S1 axons were located in relatively dorsal and ventral regions in the CC, respectively (Fig. 1*B Right*, sagittal views; 3D reconstructions are shown in Movies S1–S4).

To quantify the spatial segregation of labeled axons within the CC, we first identified the optimal segregation surface between red and green axons in the 3D space. This segregation surface then was flattened into a plane (*Materials and Methods* and realigned images in Fig. 1*A Lower Center Inset*), after which the mean fluorescence intensity was projected onto the dorsal–ventral (D–V) axis of the CC (Fig. 1*B Left*). The percentage of overlap was defined as the ratio of overlapping area to the total area of the fluorescence profiles of two axon populations (*Materials and Methods* and Fig. S1*E*), with 0% and 100% representing total segregation and total overlap, respectively. In the example shown in Fig. 1*B*, the percentages of overlap determined for sections at four different locations were in the range of 2.5–6.4%. Furthermore, when the labeled M1 and S1 regions were farther apart in the cortex, the overlap of labeled M1 and S1 axons was relatively lower (Fig. S2). The dual-labeling method also was used to examine the topography of axons originating from two adjacent S1 areas in a P8 mouse (Fig. 1*C*). Clear segregation of axons from labeled medial and lateral S1 areas along all four CC positions was observed, with the percentage of overlap higher than in M1 and S1 described above (Fig. 1*D*). Thus, CC axons derived from two adjacent cortical regions remain well segregated within the CC before and after midline crossing.

The center of the labeled cortical areas was used to represent the average somal location of labeled axons (*Materials and Methods* and Fig. S3). In total, quantitative analyses were performed for dual-labeling studies on 13 WT mice, four *Nrp1*$^{flox/flox}$ mice, and three *sema3A*$^{flox/flox}$ mice (see later description of studies using these mutant mice). We found that the percentage of overlap inversely correlated (R^2 = 0.70) with the distance between the two labeled areas regardless of genetic background (Fig. 1*E*, n = 20). This result agrees with the expectation that axons originating from more distant cortical locations are more segregated in the CC. Furthermore, we found a strong positive correlation (R^2 = 0.75) between the somal location (the center of labeled area relative to the midline) and the average position of labeled axons (the mean value; arrows in Fig. 1 *B* and *D*) relative to the dorsal surface of the CC (Fig. 1*F*). Thus, axon position within the CC is determined by the cortical location of its soma, and the topography of cortical neurons is preserved within the CC tract, with axons originating from more medial cortical areas located more dorsally.

Unlike most other nerve tracts in the nervous system, the CC contains axons from the two hemispheres projecting in opposite directions. An interesting issue is how axons from bilateral homotopic cortices are organized in the CC. We examined this issue by expressing mCherry and EGFP in the relatively homotopic regions of the two hemispheres by sequential in utero electroporation of

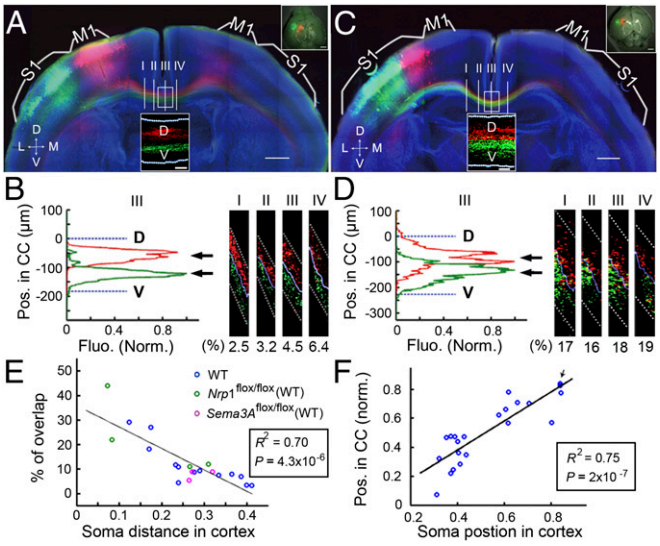

Fig. 1. Axons from different cortical regions are segregated in the CC. (*A*) A 200-μm coronal section from a P8 mouse with M1 and S1 neurons labeled with mCherry and EGFP, respectively. (*Insets*) (*Upper Right*) Images of the whole-mount cortex. (Scale bar, 500 μm.) Segregation of axons at four different locations (marked I, II, III, IV) was analyzed before and after midline crossing. (*Lower Center*) Realigned image of CC axons for section III at a higher resolution used for quantitative analysis of axon segregation within the CC. (Scale bar, 50 μm.) (See *Material and Methods* and Fig. S1) Dotted white lines demarcate dorsal and ventral surfaces of the CC. M1, primary motor cortex; S1, primary somatosensory cortex. (*B*) (*Left*) Fluorescence profiles of labeled axons at section III at various positions along the D–V axis of the CC. The profiles represent the normalized fluorescence intensity of CC axons (*Material and Methods* and Fig. S1). The percentage of overlap between two populations of axons was calculated as described in *Materials and Methods*. Arrows indicate positions of the mean value of fluorescence intensity. (*Right*) Sagittal view of four sections, with percentages of overlap shown below. (*C* and *D*) Coronal section from a P8 mouse double-labeled with mCherry and EGFP in two adjacent S1 regions. Data are presented as in *A*–*C*. (*E*) Correlation between the percentage of overlap and the distance from the center of the two labeled cortical areas (*Material and Methods* and Fig. S3). Circles of different colors are data points from 13 WT mice, four *Nrp1*$^{flox/flox}$ mice, and three *Sem3A*$^{flox/flox}$ mice, representing three types of control mice without genetic manipulation of Sema3A/Nrp1 signaling. (*F*) Correlation between the average position of the labeled axon in the CC (relative to the dorsal surface of CC) and the center of the labeled cortical area relative to the midline (n = 11 WT mice). Arrow indicates two overlapped data points. R^2, square of Pearson's correlation coefficient. *P*, statistical significance tested against the null hypothesis assuming no correlation. (Scale bars, 500 μm for all panels except *Insets*.) D, dorsal; Fluo., fluorescence; L, lateral; M, medial; Pos., position; V, ventral. The *x*-axes are the normalized soma distance (*E*) and normalized soma position (*F*) in the cortex.

vectors expressing these proteins in E15.5 embryos (*Materials and Methods*). Electroporated mouse brains were sectioned coronally (200 μm) at P8. We found that most of the axons labeled red and green were located in the same position within the CC (Fig. S4 *A Inset* and *B Right*, n = 5). The percentage of overlap was as high as 96%. In the example shown in Fig. S4, the somal locations of red axons in the cortex were slightly more lateral than those of the green axons; correspondingly the distribution of the red fluorescence axon profile along the D–V axis of the CC was more ventral than that of the green fluorescence axon profile (Fig. S4*B Left*). Thus, callosal axons from homotopic regions of the two hemispheres occupy the same location within the CC.

Dorsally Located Axons Project Medially After Midline Crossing. We next examined whether axon position within the CC contributes to the temporal order of the axon's contralateral cortical projection. Using high-resolution confocal imaging (see *Materials*

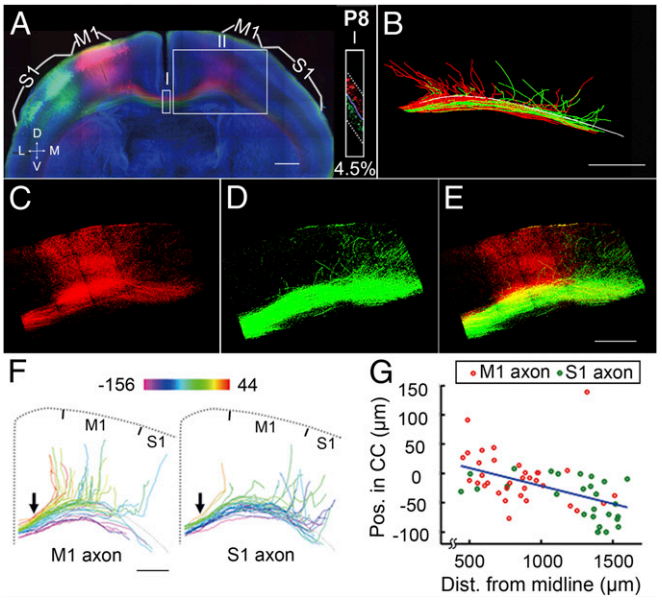

Fig. 2. Dorsally located axons in the CC project medially after midline crossing. (*A*) A 200-μm coronal section from a P8 mouse, with mCherry and EGFP labeling of M1 and S1, respectively, presented as in Fig. 1*A*. (*Inset*) Sagittal view of the area in box I at a higher resolution (percentage of overlap, 4.5%). (*B*) Tracing of axon projections to the contralateral cortex (from midline to medial S1, covering ~1.9 mm; box II in *A*). The white line indicates the dorsal CC surface. See Movie S5 for an illustration of the tracing procedure. (*C–E*) High-magnification images of box II in *A*. (*F*) Axons from M1 and S1 were color-coded by their positions within the CC (at the location marked by the arrow). Color scale shows coding of D–V position linearly from −156 to 44 μm. Position 0 is defined by the CC boundary, as revealed by Hoechst staining (*Material and Methods*). (*G*) Correlation between the axon's D–V position in the CC (location of axon's starting point at the midline) and the axon's turning point along the CC (defined by the distance from the midline). See Fig. S5 and *Material and Methods* for detailed illustration. $R^2 = 0.25$; $P = 4 \times 10^{-5}$. (Scale bar, 500 μm for all panels.) Dist., distance.

and Methods and Movie S5 for the details of the tracing method), we manually traced all identifiable individual axons of M1- and S1-labeled neurons and found that axons located more dorsally within the CC left the tract earlier after midline crossing to more medial regions of the contralateral cortex (Fig. 2 *A–E*; $n = 2$). This projection pattern became more apparent when axons from either M1 or S1 were color-coded according to their CC positions at the midline (arrows, Fig. 2*F*).

Although M1 axons located more dorsally in the CC were found to project to the contralateral M1 as expected, the axons located more ventrally in M1 often stayed within the CC, with some projecting inappropriately to S1. Similarly, some dorsally located S1 axons projected inappropriately to M1, whereas more ventrally located S1 axons mostly projected correctly to the contralateral S1. Furthermore, the distance of the axon's turning point from the midline (*Materials and Methods* and Fig. S5 *E* and *F*) correlated highly with the D–V position in the CC (Fig. 2*G*), consistent with the observation that dorsally located axons project to more medial cortical regions. Similar axonal projections were analyzed in P8 mice in which the medial and lateral S1 regions were double-labeled (Fig. S6 *A–E*). A correlation between axon position in the CC and the location of the axon's turning point was again observed (Fig. S6 *F* and *G*). Together, these results support the hypothesis that the position of the axon within the CC largely determines the timing or position of its contralateral cortical projection.

Expression Patterns of Sema3A and Nrp1. Previous studies have shown that Sema3A/Nrp1 signaling is required for axon segregation in the developing olfactory nerve (17) and for fasciculation and guidance of callosal axons (18–20, 27, 28). Using in situ hybridization (*Materials and Methods*), we found a distinct pattern of Sema3A expression that is complementary to Nrp1 expression in the cortex and other brain regions (Fig. 3 *A* and *B*). The distribution of Sema3A mRNA was widespread but discretely localized in the cortex with slightly increased signal in the lateral side of cortical region, whereas the distribution of Nrp1 mRNA showed a gradient from M1 to S1 in layer II/III neurons, consistent with the dorsal-high and ventral-low expression pattern of Nrp1 protein within the CC, as shown by immunostaining with Nrp1 antibodies (Fig. 3*C*). Hybridization signals were not detected using the respective sense probe (Fig. S7). In short, our findings are consistent with those reported by Zhao et al. (28) and Ren et al. (18). The complementary expression pattern of Sema3A and Nrp1 in Imai et al. (29) and Zhao et al. (28) support the notion that Sema3A/Nrp1 signaling could contribute to D–V ordering of axons within the CC.

Disruption of Axon Order in Sema3A-KO and *Nrp1*$^{M1-/-}$ Mice. To examine the role of Sema3A/Nrp1 signaling in the ordering of CC axons, we eliminated Sema3A expression by using Sema3A gene-deletion (KO) mice (30). Sema3A-KO embryos were electroporated with vectors expressing mCherry in M1 and EGFP in S1. Examination of coronal sections of P8 cortices from these Sema3A-KO mice showed gross defasciculation of both M1 and S1 axons within the CC (Fig. 4 *E* and *F*), with a high percentage of axonal overlap near the midline (in this case, 66%). These abnormalities were not observed in WT and heterozygous pups from the same litters (Fig. 4 *A–D*).

In addition, we also examined the role of Nrp1 in determining axon order within the CC. Embryos of floxed *Nrp1* mice (27) were electroporated in utero with vectors expressing Cre-recombinase (Cre) and EGFP into M1 and a vector expressing mCherry into S1 (*Materials and Methods*). Immunostaining of brain slices of postnatal electroporated mice showed selective Cre and GFP staining in M1 (Fig. S8*A*), demonstrating the effectiveness of Cre expression. Cre-mediated recombination between two loxP sites should result in the excision of *Nrp1* (31) and the absence of

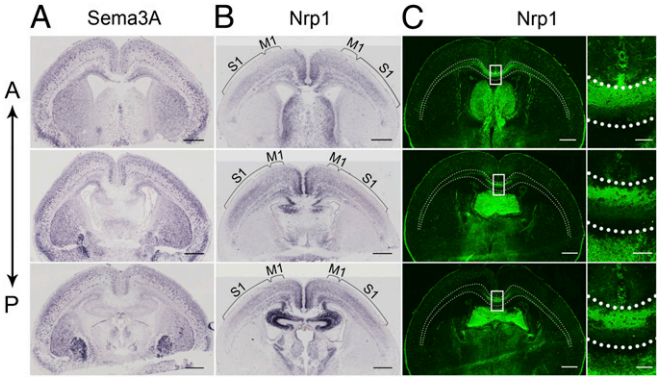

Fig. 3. Expression patterns of Sema3A and Nrp1. (*A* and *B*) Coronal sections (12-μm) from P0 WT mice showing in situ hybridization staining for Sema3A and Nrp1 mRNAs. Three sections from the same mouse are shown in the anterior (A)-to-posterior (P) sequence in each panel. Note the complementary pattern of expression for Sema3A and Nrp1 in the cortex and other brain regions in all three sections. Brackets indicate the Nrp1 mRNA gradient from M1 to S1 in layer II/III neurons. (*C*) (*Left*) Images of Nrp1 immunostaining in anterior-to-posterior sections. (*Right*) Higher-resolution images of the region within the box at the midline. (Scale bars, 100 μm.) Note dorsal-high and ventral-low expression pattern in the CC, consistent with the expression of Nrp1 mRNA. Dotted white lines indicate the CC boundary, as revealed by Hoechst staining (*Materials and Methods*). Dotted white lines indicate the CC boundary, as revealed by Hoechst staining (*Materials and Methods*). (Scale bars, 500 μm for *A*, *B*, and *C Left*.)

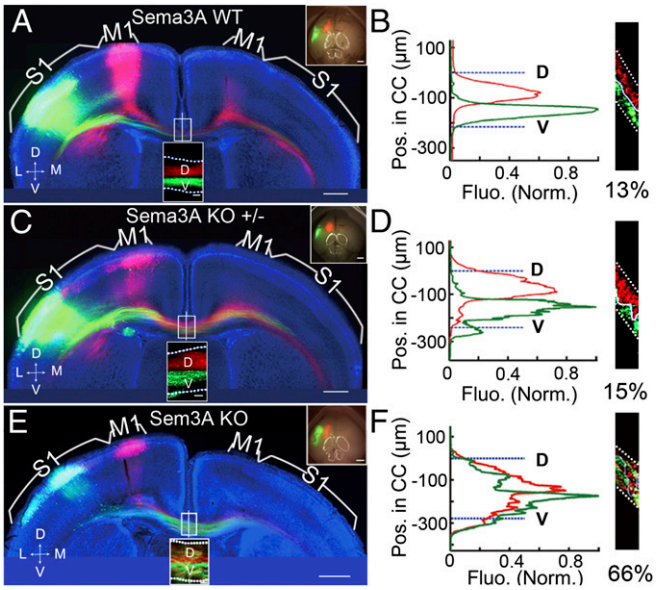

Fig. 4. Disruption of axon order in Sema3A-KO mice was specific and dosage dependent. (*A* and *B*) A 200-μm coronal section from a P8 WT mouse brain (littermate of the Sema3A KO mouse) with mCherry expression in M1 and EGFP expression in S1, presented as in Fig. 1 *A* and *B*. As shown by the mean fluorescence intensity of M1 and S1 axons along the D–V axis of the CC and the percentage of overlap at the midline, the axon order was not disrupted. (*C* and *D*) A 200-μm coronal section of the brain of a P8 Sema3A-heterozygous mouse (from the same litter as the Sema3A KO mice) with mCherry expression in M1 and EGFP expression in S1. No disruption of axon order in the CC was observed. (*E* and *F*) A 200-μm coronal section from the brain of a P8 Sema3A KO mouse with mCherry expression in M1, and EGFP expression in S1. The D–V order within the CC was grossly disrupted in the Sema3A KO mice, as shown by the mean fluorescence intensity of M1 and S1 axons along the D–V axis at the midline and the high percentage of overlap shown in *F*. (Scale bars, 500 μm in *A*, *C*, and *E*.) Dotted white lines indicate the CC border.

Nrp1 in EGFP-expressing M1 axons. This effect was confirmed by comparing the Nrp1 immunostaining in these conditional *Nrp1*-deletion ($Nrp1^{M1-/-}$) mice with that in control floxed mice from the same litter (Fig. S8 *B* and *C*). Examination of coronal sections of P8 cortices from these $Nrp1^{M1-/-}$ mice showed extensive mixing of M1 and S1 axons within the CC (Fig. 5 *D–F*) with a high percentage of overlap (41% in this case) near the midline. As controls, we observed well-segregated M1 and S1 axons when embryos of WT mice were electroporated with vectors expressing Cre/EGFP in M1 and mCherry in S1 (Fig. S9 *A* and *B*), indicating that Cre expression by itself did not affect axon segregation. Furthermore, no effect on the orderly axon segregation was observed when floxed *Nrp1* mouse embryos were electroporated with mCherry-vector in M1 and EGFP-vector in S1 (Fig. 5 *A–C*) or when floxed *Nrp1* mouse embryos were electroporated with mCherry in M1 and Cre/EGFP in S1 (Fig. S9 *C* and *D*). Thus, the disruption of axon segregation was not caused by in utero electroporation in floxed *Nrp1* mice and was observed specifically with Nrp1 deletion in M1 axons but not in S1 axons. Together, these results showed that the ordered topography of M1 axons within the CC could be attributed at least in part to their expression of Nrp1.

Given the finding that callosal axons from homotopic regions of the two hemispheres are located in the same position within the CC, we further examined whether Nrp1 expression in M1 axons also affects the order of axons from the contralateral M1 in a non–cell-autonomous fashion. To address this question, we expressed Cre together with a low concentration of EGFP in M1 of one hemisphere and expressed mCherry and EGFP in M1 and S1, respectively, in the opposite hemisphere (Fig. 5 *G–I*). The low EGFP concentration marked the location of Cre expression without labeling the CC axons (*Inset II* in Fig. 5*G*). As shown in Fig. 5*H*, we found that the order of axons from the opposite hemisphere also was severely disrupted when Nrp1 was conditionally deleted in M1 axons in one hemisphere. As controls, we expressed empty vector together with a low concentration of EGFP in M1 of one hemisphere and expressed mCherry and EGFP in M1 and S1, respectively, in the opposite hemisphere (Fig. S9*E*). We observed no severe disruption of axon order within the CC (Fig. S9*F*). Thus, the order of axons from the contralateral homotopic cortical region also contributes to the order of axons within the CC.

To quantify the results from the above experiments further and to exclude effects caused by animal-to-animal variation in the electroporation sites, we summarized a comparison graph showing the plot of percentages of overlap versus cortical distances for data from different experiments (Fig. 5*J*). In this plot, we present the data shown in Fig. 1*E*, together with additional data points obtained from $Nrp1^{M1-/-}$ mice with *Nrp1* deletion in ipsilateral ($n = 9$) and contralateral ($n = 6$) M1 and from control mice with contralateral deletion ($n = 8$). We found that the disruption of axon order in $Nrp1^{M1-/-}$ mice was dramatic in comparison with controls. This result further supports the notion that the Sema3A/Nrp1 signaling pathway plays an important role in ordering the topography of M1 axons within the CC.

Contralateral Axon Projections in Sema3A-KO and $Nrp1^{M1-/-}$ Mice. The disrupted order of M1 and S1 axons within the CC of the Sema3A-KO and $Nrp1^{M1-/-}$ mice offered an opportunity to determine whether the cortical origin of the M1 and S1 axons determines their contralateral projection after midline crossing. If the cortical origin rather than the axon position within the CC is the primary determinant of the projection, we would expect that the labeled M1 and S1 axons would project homotopically despite the disrupted D–V position of these axons within the CC.

Surprisingly, we found that extensive mixing of M1 and S1 axons within the CC of Sema3A-KO ($n = 2$) and $Nrp1^{M1-/-}$ ($n = 5$) mice led to a severe disruption of the homotopic contralateral projection (Fig. 6). Furthermore, the projection of both M1 and S1 axons still depended on their individual D–V positions within the CC, with more dorsally located axons projecting to more medial regions of the contralateral cortex and the most ventrally located axons remaining within the CC over a distance of ~2.5 mm after midline crossing (Fig. 6 *B*, *C*, *F*, and *G*). Axon position in the CC also correlated highly with the distance of the axon's turning point from the midline (Fig. 6 *D* and *H*), similar to our findings in WT mice.

Disruption of Axon Order by *Sema3A* Deletion or *Nrp1* Overexpression. As shown in Fig. 3*A*, the expression of Sema3A mRNA was ubiquitous, not only within and surrounding the CC but also in the cortical neurons. To explore further how Sema3A/Nrp1 signaling may participate in ordering axon topography within the CC, we conditionally deleted *Sema3A* in layer II/III neurons of M1 and S1 by electroporating the plasmids of Cre/EGFP into the M1 and S1, respectively, of *Sema3A* floxed mice (30) at E15.5 (Fig. 7 *A–D*). Analysis of the brain sections at P8 showed that the axon order was clearly disrupted (Fig. 7 *B* and *D*), as shown by the percentages of overlap between M1 and S1 axons in five $Sema3A^{M1-/-}$ mice and in six $Sema3A^{S1-/-}$ mice, in comparison with floxed and WT controls (Fig. 7 *E–G*). However, the disrupted phenotype was not as strong as that found in Sema3A KO mice ($n = 4$) (Fig. 7*G*), suggesting that Sema3A is required both cell autonomously and within the CC tract and is important for ordering axons in the CC.

As previously described, Nrp1 mRNA was expressed in a gradient from M1 to S1 in layer II/III neurons, consistent with the dorsal-high and ventral-low expression of Nrp1 protein within the CC (Fig. 3 *B* and *C*). To test the possibility that this gradient of Nrp1 expression may contribute to axon ordering within the CC, we performed a gain-of-function experiment by expressing plasmids

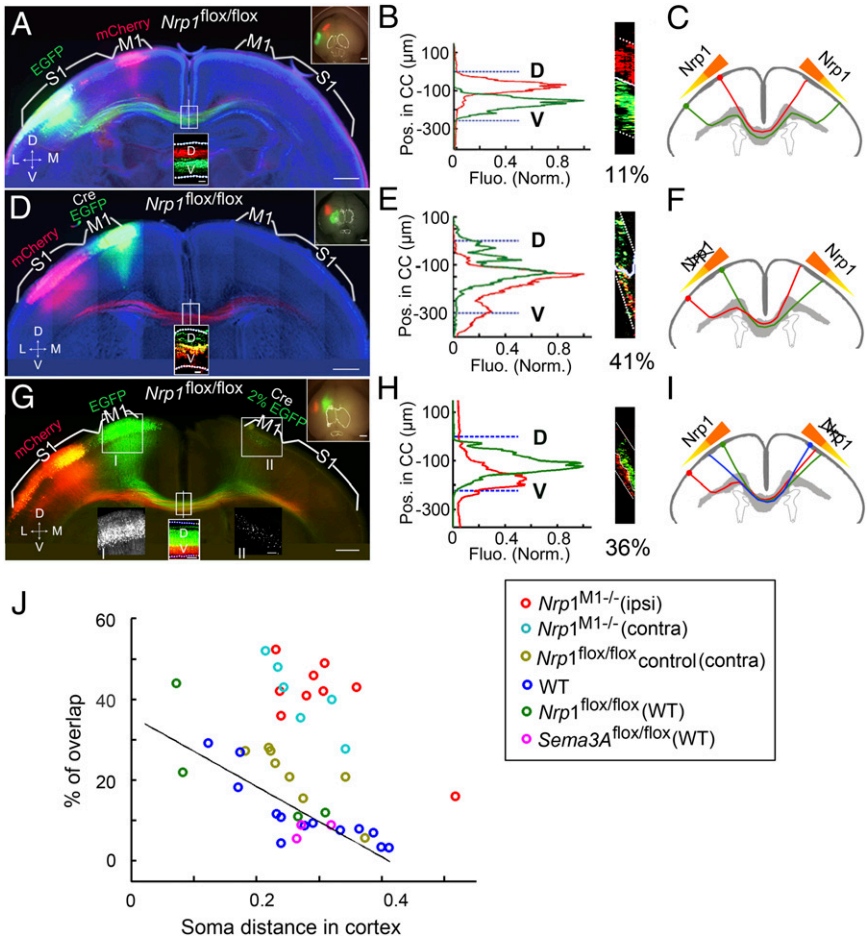

Fig. 5. Disruption of axon order in *Nrp1*$^{M1-/-}$ mice. (*A* and *B*) A 200-μm coronal section from the brain of a P8 *Nrp1*$^{flox/flox}$ mouse with mCherry expression in M1 and EGFP expression in S1. Data are presented as in Fig. 1 *A* and *B*. No disruption of axonal order was observed in the CC. (*C*) Schematic diagram of the topographical arrangement of CC axons within the CC corresponding to its contralateral cortical projection. The gradient of Nrp1 in layer II/III neurons in the cortex is in relationship with the axon order within the CC. (*D–F*) Example of a 200-μm coronal section from P8 *Nrp1*$^{M1-/-}$ mice with Cre and EGFP expression in M1 and mCherry expression in S1. Data are presented as in *A–C*. The D–V order within the CC was grossly disrupted. As shown in the schematic diagram (*F*) the axon order was disrupted when the gradient of Nrp1 was disturbed ipsilaterally, resulting in abnormal but position-dependent contralateral cortical projection. (*G–I*) Coronal section (200-μm) from P8 *Nrp1*$^{M1-/-}$ mice, with mCherry in M1 and EGFP expressed in S1 in one hemisphere and Cre expressed together with a low-level of EGFP in the contralateral homotopic M1 that labeled the cell bodies but not axons. (*Insets I* and *II*) High-magnification images areas in boxes I and II. The axon order was disrupted compared with control (Fig. S9 *E* and *F* and Fig. 5*J*). As shown in *I*, the disruption of the Nrp1 gradient disturbed the axon order in the opposite hemisphere in a non–cell-autonomous manner. (*J*) Plot of percentages of overlap versus cortical distances for data from different experiments. Data from Fig. 1*E* for control mice (WT, *Nrp1*$^{flox/flox}$, and *Sem3A*$^{flox/flox}$) are included for comparison with data from mice in which Sema3A/Nrp1 signaling was manipulated. *Nrp1*$^{M1-/-}$ (ipsi), mice with Nrp1 deletion in ipsilateral cortex (n = 9); *Nrp1*$^{M1-/-}$ (contra), mice with Nrp1 deletion in the contralateral cortex (n = 6); *Nrp1*$^{flox/flox}$ (contra), mice expressing lower level of EGFP in the contralateral M1 without Nrp1 deletion (n = 8). (Scale bars, 500 μm for *A*, *D*, and *G*.) Dotted white lines indicate the CC border.

encoding Nrp1 and EGFP in layer II/III neurons of S1 by in utero electroporation at E15.5 in WT mice (Fig. 8*G*). We found that the axon order was severely disrupted in brain sections of P8 mice (n = 7) compared with control mice of the same litter (Fig. 8 *A* and *M*). The data for the percentage of overlap are shown in Fig. 8*M*. These results, together with the results from *Nrp1*$^{M1-/-}$ mice (Fig. 5 *D–J*), suggest that Nrp1 signaling participates in establishing the axon order within the CC. Furthermore, we overexpressed Nrp1 in the layer II/III neurons of M1 in WT mice, where Nrp1 is expressed at a relatively high level (Fig. 8*D*), and found that the axon order was normal (Fig. 8 *E* and *F*), suggesting that the high level of native Nrp1 already may have exerted the maximal action on the axon order.

As shown in Fig. 5 *G–J*, the order of M1 axons within the CC was disrupted by the order of contralateral M1 axons. We performed additional experiments showing that the order of S1 axons also was affected by contralateral S1 axons, using overexpression of Nrp1 together with a low concentration of EGFP in S1 of one hemisphere, and mCherry and EGFP expression in the contralateral M1 and S1 (Fig. 8 *J–M*). Taken together, these results further support the notion that Sema3A/Nrp1 signaling is critical for the topographic ordering of cortical axons within the CC.

Developmental Refinement Failed to Eliminate Heterotopic Projections in *Nrp1*$^{M1-/-}$ Mice. In WT mice, a small population of M1 and S1 axons are known to project inappropriately to heterotopic cortices during early development, but these inappropriate projections are pruned later in development by activity-dependent mechanisms (24, 32–36). In the present study, we indeed observed a small population of heterotopic projections of S1 axons to the contralateral M1 in P8 WT mice, and vice versa (Fig. 2). However, with the exception of a few axons, most heterotopic projections in mature WT mice were eliminated by P30 (Fig. 9 *A–D*), consistent with previous reports (37–39). In contrast, a large number of

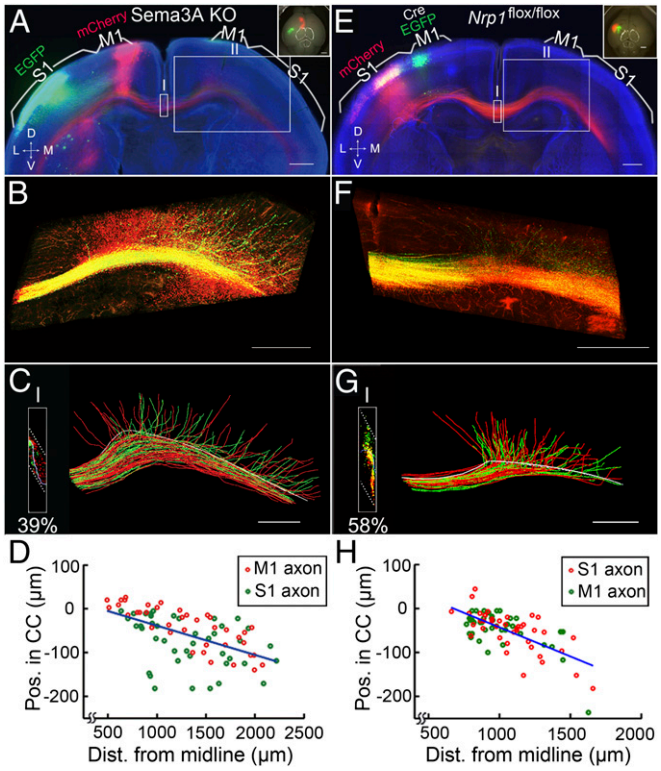

Fig. 6. Contralateral axon projection in Sema3A-KO and $Nrp1^{M1-/-}$ mice. (*A*) A 200-μm coronal section from the brain of a P8 Sema3A-KO mouse with mCherry expressed in M1 and EGFP expressed in S1, presented as in Fig. 1*A*. The axon order in the CC was grossly disrupted. (*B*) High-magnification images of axon projections in the contralateral hemisphere (box II in *A*). (*C*) Tracing of axon projections from midline to the contralateral medial S1 (~2.5 mm; box II in *A*). (*Inset*) High percentage of overlapping in the CC (39%) at the midline (box I in *A*). (*D*) Correlation between axon's D–V position in the CC and the axon's turning point along the CC. $R^2 = 0.31$, $P = 8 \times 10^{-8}$. (*E*–*H*) A 200-μm coronal section from the brain of a P8 $Nrp1^{M1-/-}$ mouse with Cre/EGFP expressed in M1 and mCherry expressed in S1. Data are presented as in *A*–*D*. In *H*, $R^2 = 0.45$, $P = 8 \times 10^{-12}$. (Scale bars, 500 μm.)

heterotopic contralateral projections persisted in P30 $Nrp1^{M1-/-}$ mice even though developmental refinement had reduced some of the heterotopic projections found in P8 $Nrp1^{M1-/-}$ mice (Fig. 9 *E*–*H*, $n = 2$).

The finding that aberrant heterotopic projections persisted in mutant mice indicates that disruption of the axon order within the CC in early development results in severe defects in their contralateral projections that cannot be corrected by later developmental pruning. Thus, initial axon position-dependent projection is critical for the development of homotopic mapping of CC axons.

Discussion

In this study, we found that axons from different cortical regions are arranged in a topographically ordered manner within the CC, before their projection into their corresponding contralateral cortical area. Previous studies using fluorescent carbocyanine dye (DiI) labeling of two distant cortical regions in separate mice already have suggested that axons from medial and lateral regions occupy dorsal and ventral positions within the CC, respectively (20, 40). By dual labeling of cortical neurons in two defined cortical regions with the in utero electroporation method and quantitative image analysis of axon distribution at a high resolution over large areas, we now demonstrate that the topography of cortical neurons is tightly constrained by the D–V position of their axons within the CC. Importantly, we further show that the axon position within the CC determines the timing of its projection to the contralateral cortex after midline crossing, with more dorsally located axons projected earlier. To test further the importance of the order of axons in the CC in their projection pattern, we disrupted the axon order by five different genetic manipulations: (*i*) deletion of Nrp1 in a subpopulation of M1 neurons; (*ii*) overexpressing Nrp1 in a subpopulation of S1 neurons; (*iii*) deletion of Sema3A in a subpopulation of M1 neurons; (*iv*) deletion of Sema3A in a subpopulation of S1 neurons; and (*v*) deletion of Sema3A in the entire brain. These manipulations resulted in a disruption of axon order in the CC, as indicated by markedly increased overlapping of M1 and S1 axons within the CC, suggesting the importance of the Sema3A/Nrp1 signaling in the topographic order of axons in the CC. There are well-documented effects of Sema3A/Nrp1 signaling in the guidance of neuronal migration and axon growth, which we also observed in the present studies (Fig. S10*B*). However, despite

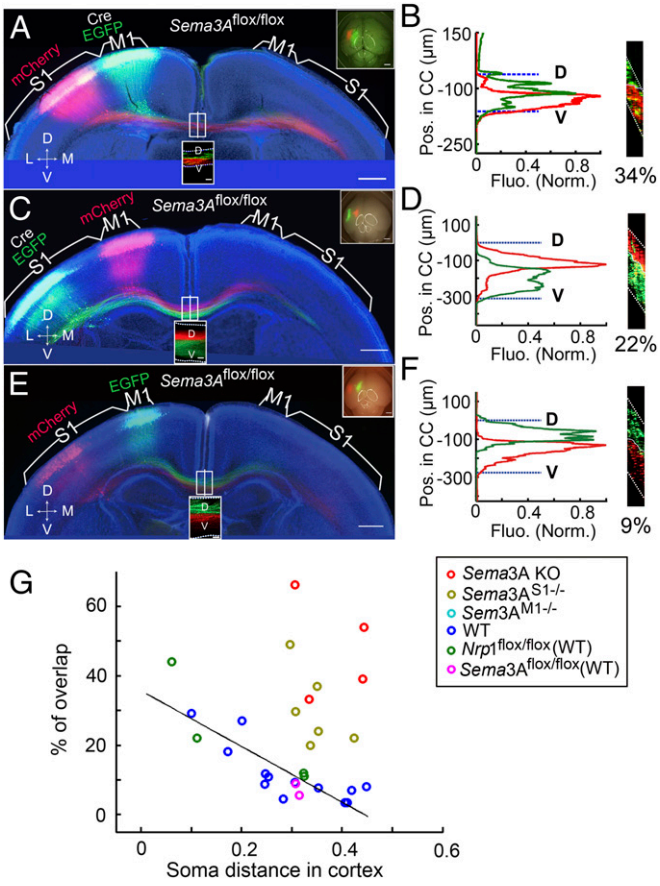

Fig. 7. Disruption of axon order in $Sema3A^{M1-/-}$ and $Sema3A^{S1-/-}$ mice. (*A* and *B*) A 200-μm coronal section from the brain of a P8 $Sema3A^{M1-/-}$ mouse with Cre and EGFP expressed in M1 and mCherry expressed in S1, presented as in Fig. 1 *A* and *B*. The D–V axon order within the CC was disrupted, as shown by the fluorescence profiles of labeled axons in *B* for the section at the midline in *A* projected along the D–V axis of the CC. (*C* and *D*) A 200-μm coronal section from the brain of a P8 $Sema3A^{S1-/-}$ mouse with mCherry expressed in M1 and Cre and EGFP expressed in S1. Data are presented as in *A* and *B*. The D–V order within the CC also was disrupted in this mouse. (*E* and *F*) A 200-μm coronal section from the brain of a P8 $Sema3A^{S1-/-}$ mouse with EGFP expressed in M1 and mCherry expressed in S1, presented as in *A* and *B*. The D–V order within the CC was normal. (*G*) Plot of percentages of overlap versus cortical distances from experiments using Sema3A KO mice ($n = 4$) and mice with conditional Sema3A deletion in M1 ($Sema3A^{M1-/-}$) ($n = 5$) or in S1 ($Sema3A^{S1-/-}$) ($n = 6$), together with data from control mice shown in Fig. 1*E*. (Scale bars, 500 μm in *A*, *C*, and *E*.)

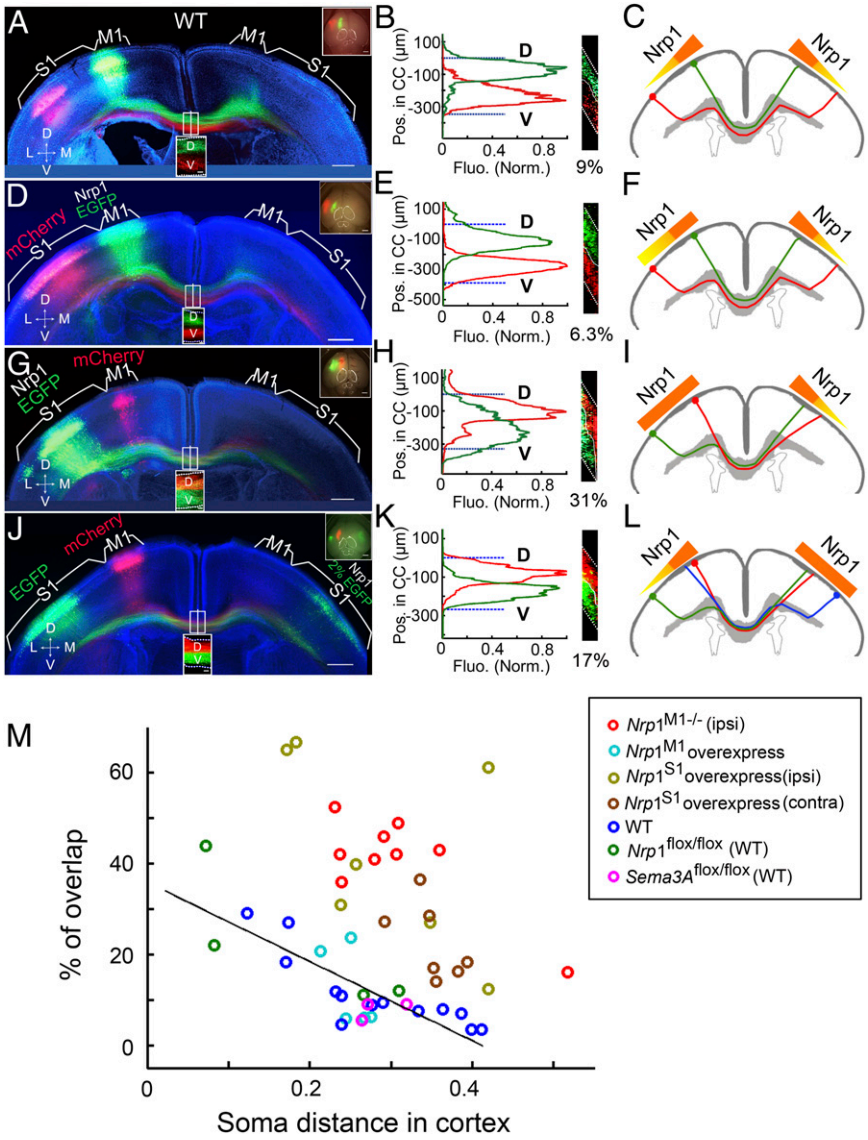

Fig. 8. Disruption of axon order in mice overexpressing *Nrp1*. (*A–C*) A 200-μm coronal section from the brain of a P8 mouse with EGFP expressed in M1 and mCherry expressed in S1. Data are presented as in Fig. 5 *A–C*. No disruption of the axonal order was observed in the CC. (*D–F*) A 200-μm coronal section from the brain of a P8 mouse with overexpression of Nrp1 and EGFP in M1 and mCherry in S1. Data are presented as in *A–C*. The D–V order within the CC was normal. As the schematic diagram (*F*) shows, although Nrp1 was overexpressed in M1, the gross Nrp1 gradient was not disrupted; therefore the axon order within the CC was normal. (*G–I*) A 200-μm coronal section from the brain of a P8 mouse with mCherry expression in M1 and overexpression of Nrp1 and EGFP in S1. As the schematic diagram (*I*) shows, the overexpression of Nrp1 in S1 affected the medial–lateral Nrp1 gradient in the cortex, so the axon order within the CC was grossly disrupted. (*J–L*) A 200-μm coronal section from the brain of a P8 mouse with expression of mCherry in M1 and EGFP in S1 in one hemisphere and overexpression of Nrp1 together with low-level expression of EGFP in the contralateral homotopic S1 that labeled the cell bodies but not axons. The axon order was disrupted compared with WT control (Fig. 8 *A–B*). As the schematic diagram (*L*) shows, the abnormal axon order of the contralateral cortex resulting from the disruption of the Nrp1 gradient disrupted the axon order in the opposite hemisphere in a non–cell-autonomous manner. (*M*) Summary of percentages of overlap in mice with Nrp1 deletion in M1 [$Nrp1^{M1-/-}$ (ipsi)] ($n = 9$) and mice with Nrp1 overexpression in M1 ($Nrp1^{M1}$, $n = 5$) or S1 [$Nrp1^{S1}$, $n = 7$; $Nrp1^{S1}$(contra), $n = 7$]. (Scale bar, 500 μm for *A*, *D*, *G*, and *J*.)

the abnormal phenotypes in neuronal migration and axon growth, we found that in genetically manipulated mice with defective Sema3A/Nrp1 signaling a substantial number of axons still entered the CC tract and projected to the contralateral cortices (Fig. S10). Thus we were able to observe the effect of disrupting axon order in contralateral projection.

The main finding of the present study is that the contralateral cortical projection of misplaced axons within the CC remains strictly dependent on their D–V position within the CC. This dependence resulted in many aberrant projections of S1 axons in the contralateral M1 that could not be corrected by developmental refinement by P30. Because the initial contralateral projection depends on the axonal position regardless of the cortical origin of the axon, axons from different cortical origins possess the same capability of responding to turning cues present in different cortical regions.

Mechanisms for CC Axon Order and Position-Dependent Turning. During development, surrounding glia structures at the midline establish the boundary of the callosal tract by acting as a source of guidance cues to prevent axons from leaving the tract and entering the adjacent structures (41). Many guidance cues and their re-

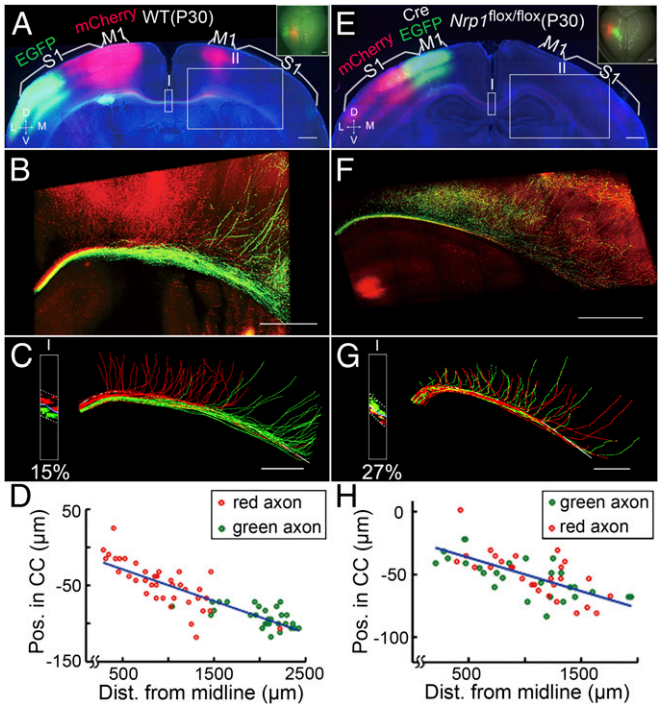

Fig. 9. Developmental refinement failed to eliminate heterotopic projections in $Nrp1^{M1-/-}$ mice. (*A*) Coronal section from a WT P30 mouse with mCherry expression in M1 and EGFP expression in S1, presented as in Fig. 1*A*. (*B*) High-magnification image of axon projection in the contralateral cortices (box II in *A*). (*C*) Tracing of axon projections from the midline to the contralateral medial S1 (~2.5 mm, box II in *B*). (*Inset*) Fluorescence profile at the midline (box I, in *A*; percentage of overlap, 15%). The white line shows the dorsal surface of the CC. Note that nearly all nonhomotopic projections were pruned. (*D*) Correlation between the axon's D–V position within the CC and the axon's turning point along the CC. $R^2 = 0.73$, $P = 2 \times 10^{-20}$. (*E–H*) Coronal section from a P30 $Nrp1^{M1-/-}$ mouse, with Cre/EGFP expression in M1 and mCherry expression in S1. Data are presented as in *A–D*. Note that although many of nonhomotopic projections were pruned compared with those in the P8 $Nrp1^{M1-/-}$ mouse (Fig. 6), a large number of nonhomotopic contralateral cortical projections remained. Importantly, the correlation between the axon's D–V position in the CC and its turning point was maintained. $R^2 = 0.47$, $P = 6.7 \times 10^{-9}$. (Scale bars, 500 μm.)

ceptors are found to be expressed in the midline region, including ephrins/ephrin receptors (Ephs) (21, 42), semaphorins/Nrp1 (19), Netrin/deleted in colorectal cancer (DCC) (43), Draxin (44), Slit/Roundabout (Robo) (11, 45, 46), wingless-related MMTV integration site 5A (Wnt5A)/receptor-like tyrosine kinase (Ryk) (47), and Tsukushi (48). Concerted actions of many of these guidance cues are likely to be involved in regulating the formation of the CC before midline crossing and dispersal of axon projections to the contralateral cortices. Repulsive guidance cues provided by surrounding glial structures help confine the axons expressing the corresponding receptors within the CC tract. For example, when Slit/Robo signaling is disrupted, axons do not cross midline but project ventrally into septum (45). Secreted semaphorins are known to serve as repulsive or attractive axon guidance cues and to maintain axon bundling by preventing axon defasciculation (49); e.g., semaphorin3C (Sema3C) is expressed within the CC near the midline and serves as an attractant for cortical axons in vitro (20, 50). Furthermore, the repulsive action of Sema3A and the attractive action of Sema3C could act together near the midline to confine and maintain the order of Nrp1-expressing CC axons. In $Nrp1^{sema}$ mice, a knock-in mouse line in which Nrp1 is unable to bind semaphorins, the cingulate pioneering axons that initiate CC development project ectopically to the septum (19).

In Sema3C-KO mice, the dorsal and ventral callosal axons intermix and form ectopic axonal Probst bundles at the midline (20). In the present study we confirmed that there is a dorsal-high and ventral-low pattern of Nrp1 expression within the CC (Fig. 3*C*). If we increased the absolute concentration of Nrp1 in the dorsal CC axons without changing the expression gradient within the CC, the axon order was not disrupted and was normal compared with the WT controls (Fig. 8 *A–F*). However, if the gradient was disturbed by overexpression of Nrp1 in layer II/III neurons in S1, the axon order within the CC was severely disrupted (Fig. 8 *G–I*). In the present study, we also confirmed a distinct pattern of Sema3A expression that is complementary to Nrp1 expression in the cortex and other brain regions (Fig. 3 *A* and *B*). The distribution of Sema3A mRNA was widespread but discretely localized in the cortex with slightly increased signal in the lateral side of cortical region (Fig. 3*A*). If the Sem3A was conditionally deleted in layer II/III neurons in either M1 or S1, the axon order within the CC was disrupted (Fig. 7 *A–G*), although the phenotype was not as severe as that in the Sema3A-KO mice (Fig. 4 *E–F*). Because electroporation of Cre affects only a subset of cortical neurons, Sema3A secreted by non-electroporated neurons may help reduce the defect in axon order. Thus, the orderly confinement of the CC axons near the midline could result from the repulsive action of Sema3A secreted by the regions complementary to Nrp1 expression in the cortex and within the CC (Figs. 3, 7, and 8). The contribution from Sema3C secreted by cells within the CC also has been shown to guide the bundling of CC axons (20). In addition, ephrin receptor A also is expressed in the ventral CC axons (20, 40), suggesting that ephrin/Eph signaling also may play a role in maintaining the axon order within the CC.

Our studies of genetic manipulations showed that Sema3A/Nrp1 signaling contributes to the topographic order of axons within the CC but is not involved in the axon position-dependent projection to the contralateral hemisphere. The latter order appears to depend on attractive guidance cues derived from the contralateral cortices that are nonspecific to M1 and S1. The progressive turning of these axons in a D–V order can be attributed to the action of such attractive guidance cues, together with a progressive decrease of the physical constraint imposed by more dorsal axons that have left the CC tract.

Development of Homotopic Contralateral Projections. The formation of topographically ordered neuronal connections in the brain depends on the guidance of growing axons before their contact with the target tissue, the recognition of specific target cells by the axon, and activity-dependent stabilization and pruning of selective connections (32, 33). Our study suggests that guidance cues with complementary expression patterns within and surrounding the CC play a significant role in establishing the D–V position of axons within the CC. This ordering is analogous to the axon order observed in the olfactory nerve, where the guidance cues within and surrounding the olfactory nerve are essential for maintaining the correct axon topography and for ordered axon projection to the olfactory bulb (17, 29). The complementary expression pattern of guidance cues within the thalamocortical tracts and along their routes (12–14) before their arrival in the cortex also contributes to the correct axon organization within the thalamocortical tract and the orderly projection of thalamocortical axons to the cortex. Here we show that axon position-dependent projection is important for interhemispheric connectivity of the cerebral cortex. It is interesting that we found that the order of axons from contralateral homotopic cortices also contributes to the order of axons within the CC, because disrupting the order of ipsilateral M1 axons by deleting Nrp1 expression affected the order of axons from the contralateral M1 within the CC (Fig. 5 *G–I*), and disrupting the

order of ipsilateral S1 by overexpressing Nrp1 affected the order of contralateral S1 within the CC (Fig. 8 *J–M*). This non–cell-autonomous effect of Nrp1 deletion could be an indirect effect mediated by homophilic adhesion among axons of homotopic cortices. The nature of such cortical region-specific homophilic adhesion remains to be elucidated. Thus, axon order in the CC depends on many factors—molecular gradients of repulsive and attractive nature as well as homophilic adhesion among axons from the same or homotopic cortical region—with a net action that specify the axon's D–V position.

Our study also showed that the initial callosal axon projections in early postnatal mice are not strictly homotopic. There are minor ectopic projections of S1 axons into M1 and vice versa in P8 mice (Fig. 2*F*), most of which were eliminated at a later stage (P30) (Fig. 9 *A–D*), consistent with developmental pruning of inappropriate projections (33) through activity-dependent mechanisms (24, 32, 34–36). However, the large number of ectopic projections induced by disrupting the normal axon order within the CC in *Nrp1*$^{M1-/-}$ mutant mice in early development could not be corrected by later pruning processes (P30) (Fig. 9 *E–H*), perhaps because of the limited capability of the activity-dependent pruning mechanism. It also is possible that complete pruning of massive ectopic projections requires a much longer period beyond P30. In any case, an initially correct axon order within the CC is critical for the timely development of homotopic projections of CC axons.

Materials and Methods

Animal and Constructs. Mice were used according to a protocol approved by the Institute of Neuroscience (ION), Shanghai Institutes of Biological Sciences, Chinese Academy of Sciences (CAS). Pregnant WT mice were maintained on a mixed C57BL/6 and CBA background. *Nrp1* floxed mice (27) were a gift from Alex Kolodkin (The Johns Hopkins University, Baltimore, MD). Sema3A lacZ knock-in mice and *Sema3A* floxed mice (30) were purchased from RIKEN BioResource Center. Plasmids of ubiquitin-EGFP, ubiquitin-mCherry, and ubiqutin-Cre-2A-GFP were gifts from Z.-l. Qiu (ION, CAS). *Nrp1* sequences (51) were a gift from Stephen Strittmatter (Yale University, New Haven, CT) and were cloned into the backbone of pCAGGS.

In Utero Electroporation. After anesthesia with 0.7% (wt/vol) sodium pentobarbital, pregnant mice at E15.5 were subjected to abdominal incision to expose the uterus (52). The first plasmid was injected through the uterine wall into the medial region of the lateral ventricle of the brain with a glass pipette. Electrical pulses then were delivered to embryos by electrodes connected to a square-pulse generator CUY21 (Bex Co., Ltd). For targeting M1, the electrodes were applied at a 0° angle with respect to the rostral–caudal axis of the head. For targeting S1, the angle was 30–45°. For each electroporation, five 35-V pulses of 50 ms were applied at 1-s intervals. The second electroporation was carried out 30 min after the first. After the electroporation, the uterus was returned to the abdominal cavity, followed by suturing of the abdominal wall and skin. Pups were reared to different postnatal stages after birth.

Slice Preparation and Imaging. Under deep anesthesia, mice brains were perfused with saline followed by 4% (wt/vol) paraformaldehyde in PBS, pH7.4, and were preserved for 2 d before being placed in 20% (wt/vol) sucrose solution. The brain then was cut into 200-μm sections with a vibrating-blade microtome (Leica VT1200S). Sections first were imaged by a fluorescence microscope (Nikon E600FN or TE2000) equipped with Plan Apo 10× objective to obtain an image over a large area. Images also were acquired at a higher resolution and were assembled over a large area of the brain sections by using confocal microscopes (Zeiss 710, Leica Sp5, or Nikon A1R, 40×, NA 1.30 or 1.25). The excitation wavelengths used were (in nm) 405 (Hoechst), 488 (GFP), and 561 (mCherry).

Identification of Cortical Regions. Sections were counterstained with Hoechst 33258 (Sigma/flu/Ald) (Fig. S11*A*). S1 was identified by the presence of its barrel structure, and M1 was identified as a more medial area adjacent to S1 (Fig. S11 *B–D*), aided by the use of a atlas of the developing mouse brain (53). The dorsal and ventral surfaces of the CC were identified by an increase in cell density surrounding the white matter, as revealed by the Hoechst staining.

Analysis of Axon Segregation. To analyze and visualize the axon organization quantitatively within the CC, we performed the following procedures for each dataset obtained from the 200-μm coronal sections.

Preprocessing. A raw dataset was obtained as a series of *Z*-stack red and green fluorescence images (*x*-axis: medial–lateral, *y*-axis: D–V, *z*-axis: anterior–posterior). The resolution of both *x*- and *y*-axes was first down sampled to be the same as that of the *z*-axis by bilinear interpolation. Fig. S1*A* shows an example of a rescaled image in two different views.

Determination of the optimal segregation surface between red and green axons. First, we divided the CC into square columns along the *y*-axis (Fig. S1*B*), with the width of the column in the range of 2.0–3.2 μm (depending on the image resolution), and computed the optimal segregation plane of each column for the red and green axons by minimizing the total red and green fluorescence intensities that fell beyond the segregation plane. All the segregation planes then were assembled into the optimal separation surface, which was smoothed by median filtering with a window size ranging from 14–22 μm for different samples. The segregation surface is depicted in blue and is shown in three different views in Fig. S1*C*.

Quantitation of axon segregation. To examine the segregation along the CC (*x*-axis), we summed the fluorescence intensities along the anterior–posterior (*z*) axis after shifting the image within each column along the *y*-axis to flatten the segregation surface into a plane (Fig. S1*D*). The fluorescence intensities along the *x*-axis then were summed to obtain the fluorescence profile along the D–V (*y*) axis (Fig. S1*E*). The profile was normalized in three steps: First, the average intensities of fluorescence for two sets of labeled axons were set to be equal. Second, the final values of fluorescence at various CC positions were normalized by setting the maximal value of fluorescence for both sets of labeled axons to be 1. Finally, we defined the percentage of overlap as (overlap area/total area) × 100. (The overlap area is shown in gray, and the total area is shown by the dashed lines in Fig. S1*E*.)

Analysis of the Average Somal Position of Labeled Neurons. With the Image J software we obtained the center of mass of cell bodies by measuring the fluorescence intensity along the medial–lateral axis (dashed lines in c and d in Fig. S3). The distance along the cortex from the midline to the center of mass was defined as the average somal position of labeled axons and normalized by the size of the cortical section (Fig. S3).

Analysis of the Distribution of Labeled Callosal Axons from Two Hemispheres in the CC. The analysis was similar to that described in *Material and Methods*, *Analysis of Axon Segregation* except for steps 2 and 3. After preprocessing, images were projected along the average line of the upper and lower CC border along the *z*-axis (anterior–posterior axis) (Fig. S4*A Inset*). The fluorescence intensities along the *x*-axis then were summed to obtain the fluorescence profile along the D–V (*y*) axis (Fig. S4*B Left*).

Axon Tracing. To investigate the relationship between axon position in the CC and its contralateral projection in the target cortex, we performed the following procedures for each dataset obtained from a 200-μm coronal section.

Stitching. A raw dataset was a series of *z*-stack red and green fluorescent images. Based on the 3% overlap of two nearby stacks, data were stitched into an overall picture. This process was done using a confocal microscope (Zeiss 710 or Leica Sp5). The image resolution was 0.35 μm per pixel (Zeiss 710) or 0.38 μm per pixel (Leica Sp5). The *Z* step is 0.8 μm. The diameter of the CC axon varied from two to five pixels at P8 and from five to six pixels at P3, with no apparent difference between WT and Sema3A/Nrp1 KO mice. At the *Z* step of 0.8 μm, the same segment of the CC axon could be captured by at least three adjacent *Z* steps; therefore we chose this *Z* resolution for our tracing (to minimize bleaching of fluorescence). 3D reconstruction of axon projection images was made for up to 200 sections, allowing continuous tracing of axon projections as shown in the figures.

Manual tracing. The stitched 3D images were traced manually using the software Neurolucida 9.0. The software presents only one section at a time, and adjustment of image contrast is required for each optical section to trace axons across sections. This tracing was not possible at regions where stained axons are clustered in bundles. As an indication of the effort required to tracing an individual axon, normally ~30 min was required for completing the tracing of one single axon. This manual tracing procedure is illustrated by the Movie S5.

Analysis of the tracing data. To determine the axon position in 3D relative to the dorsal surface of the CC, we identified the dorsal surface of CC according to changes in Hoechst staining across the border (blue lines in Fig. S5 *B* and *C*). The CC borders of different sections then were aligned to the same plane to estimate the axon position in the CC along the rostral–caudal axis (Fig. S5 *A–C*). Thus, according to axon positions at the midline, we obtained a color-coded

projection pattern (Fig. 2*F* and Fig. S6*F*). To determine the distance from the midline, the border was straightened to a line, so that the positions of axons along the medial–lateral axis could be compared (Fig. S5*D*). The turning point of the axon was defined by the intersection point of two lines representing the original and the projected directions of the axon (Fig. S5 *E* and *F*).

In Situ Hybridization. Brains were removed from P0 mice after anesthesia on ice and were fixed in 4% (wt/vol) paraformaldehyde. Coronal sections of 12 μm were cut using a cryostat microtome after brains were dehydrated by 20% (wt/vol) sucrose solution. In situ hybridization was performed as previously described (54). In situ hybridization probes for *Sema3A* and *Nrp1* were the same as those used by Chen et al. (55) and were a gift from X.-b. Yuan (ION, CAS).

Immunostaining. Brains were removed from mouse pups after anesthesia on ice and were frozen rapidly in liquid nitrogen. Coronal sections of 12 μm were cut on a cryostat microtome (MICROM International GmbH, HM525) and were fixed in acetone for 10 min. Nonspecific binding was blocked by adding 5% normal goat/donkey serum during preincubation and incubation in 1× PBS containing 0.05% (vol/vol) Tween-20. The following primary antibodies were used: Nrp1 (AF566; R&D Systems). For immunostaining of Cre-recombinase (MAB3120; Millipore) and GFP (A11122; Invitrogen), brains electroporated with plasmid of Cre-2A-GFP were removed from pups and fixed in 4% (wt/vol) paraformaldehyde. Coronal sections of 50 μm were cut using a cryostat microtome after brains were dehydrated by 20% (wt/vol) sucrose solution. Sections were imaged with confocal microscopy (Nikon A1R, Plan Apo VC 60× oil objective with NA 1.4).

ACKNOWLEDGMENTS. We thank Drs. Y. Dan for suggestion on data analysis, A. Kolodkin and X.-b. Yuan for providing the floxed *Nrp1* mice, Takeshi Yagi and X.-b.Yuan for providing the Sema3A KO mice and floxed *sem3A* mice, Z.-l. Qiu for providing plasmids, Stephen Strittmatter for providing *Nrp1* plasmid, Q. Hu for technical support in confocal microscopy and data analysis, G.-q.Bi and Xu Wu for the use of microscopy facilities, and L.-p. Cheng for help in the experiment of in situ hybridization. We thank Rowan Tweedale for comments on the manuscript. This work was supported by the 973 Program (2011CBA00400) and the Strategic Priority Research Program of the Chinese Academy of Sciences (XDB02020001). L.J.R. is supported by a Principal Research Fellowship from the National Health and Medical Research Council, Australia.

1. Wise SP (1975) The laminar organization of certain afferent and efferent fiber systems in the rat somatosensory cortex. *Brain Res* 90(1):139–142.
2. Witelson SF (1985) The brain connection: The corpus callosum is larger in left-handers. *Science* 229(4714):665–668.
3. Gazzaniga MS, Bogen JE, Sperry RW (1962) Some functional effects of sectioning the cerebral commissures in man. *Proc Natl Acad Sci USA* 48:1765–1769.
4. Gazzaniga MS (2000) Cerebral specialization and interhemispheric communication: Does the corpus callosum enable the human condition? *Brain* 123(Pt 7):1293–1326.
5. Bloom JS, Hynd GW (2005) The role of the corpus callosum in interhemispheric transfer of information: Excitation or inhibition? *Neuropsychol Rev* 15(2):59–71.
6. Paul LK, et al. (2007) Agenesis of the corpus callosum: Genetic, developmental and functional aspects of connectivity. *Nat Rev Neurosci* 8(4):287–299.
7. Geschwind N, Galaburda AM (1985) Cerebral lateralization. Biological mechanisms, associations, and pathology: I. A hypothesis and a program for research. *Arch Neurol* 42(5):428–459.
8. Hynd GW, et al. (1995) Dyslexia and corpus callosum morphology. *Arch Neurol* 52(1): 32–38.
9. Udin SB, Fawcett JW (1988) Formation of topographic maps. *Annu Rev Neurosci* 11: 289–327.
10. Geschwind N (1979) Specializations of the human brain. *Sci Am* 241(3):180–199.
11. Bagri A, et al. (2002) Slit proteins prevent midline crossing and determine the dorsoventral position of major axonal pathways in the mammalian forebrain. *Neuron* 33(2):233–248.
12. Dufour A, et al. (2003) Area specificity and topography of thalamocortical projections are controlled by ephrin/Eph genes. *Neuron* 39(3):453–465.
13. Bielle F, et al. (2011) Emergent growth cone responses to combinations of Slit1 and Netrin 1 in thalamocortical axon topography. *Curr Biol* 21(20):1748–1755.
14. Powell AW, Sassa T, Wu Y, Tessier-Lavigne M, Polleux F (2008) Topography of thalamic projections requires attractive and repulsive functions of Netrin-1 in the ventral telencephalon. *PLoS Biol* 6(5):e116.
15. Sperry RW (1963) Chemoaffinity in the Orderly Growth of Nerve Fiber Patterns and Connections. *Proc Natl Acad Sci USA* 50:703–710.
16. Scholes JH (1979) Nerve fibre topography in the retinal projection to the tectum. *Nature* 278(5705):620–624.
17. Imai T, et al. (2009) Pre-target axon sorting establishes the neural map topography. *Science* 325(5940):585–590.
18. Ren T, et al. (2006) Imaging, anatomical, and molecular analysis of callosal formation in the developing human fetal brain. *Anat Rec A Discov Mol Cell Evol Biol* 288(2):191–204.
19. Piper M, et al. (2009) Neuropilin 1-Sema signaling regulates crossing of cingulate pioneering axons during development of the corpus callosum. *Cereb Cortex* 19(Suppl 1): i11–i21.
20. Niquille M, et al. (2009) Transient neuronal populations are required to guide callosal axons: A role for semaphorin 3C. *PLoS Biol* 7(10):e1000230.
21. Mendes SW, Henkemeyer M, Liebl DJ (2006) Multiple Eph receptors and B-class ephrins regulate midline crossing of corpus callosum fibers in the developing mouse forebrain. *J Neurosci* 26(3):882–892.
22. Ivy GO, Killackey HP (1982) Ontogenetic changes in the projections of neocortical neurons. *J Neurosci* 2(6):735–743.
23. O'Leary DD, Stanfield BB, Cowan WM (1981) Evidence that the early postnatal restriction of the cells of origin of the callosal projection is due to the elimination of axonal collaterals rather than to the death of neurons. *Brain Res* 227(4):607–617.
24. Innocenti GM, Price DJ (2005) Exuberance in the development of cortical networks. *Nat Rev Neurosci* 6(12):955–965.
25. Wise SP, Jones EG; SP W & EG J (1976) The organization and postnatal development of the commissural projection of the rat somatic sensory cortex. *J Comp Neurol* 168(3): 313–343.
26. Fame RM, MacDonald JL, Macklis JD (2011) Development, specification, and diversity of callosal projection neurons. *Trends Neurosci* 34(1):41–50.
27. Gu C, et al. (2003) Neuropilin-1 conveys semaphorin and VEGF signaling during neural and cardiovascular development. *Dev Cell* 5(1):45–57.
28. Zhao H, et al. (2011) A molecular mechanism that regulates medially oriented axonal growth of upper layer neurons in the developing neocortex. *J Comp Neurol* 519(5): 834–848.
29. Imai T, Sakano H, Vosshall LB (2010) Topographic mapping—the olfactory system. *Cold Spring Harb Perspect Biol* 2(8):a001776.
30. Taniguchi M, et al. (1997) Disruption of semaphorin III/D gene causes severe abnormality in peripheral nerve projection. *Neuron* 19(3):519–530.
31. Sauer B (1998) Inducible gene targeting in mice using the Cre/lox system. *Methods* 14(4):381–392.
32. McLaughlin T, O'Leary DD (2005) Molecular gradients and development of retinotopic maps. *Annu Rev Neurosci* 28:327–355.
33. Luo L, O'Leary DD (2005) Axon retraction and degeneration in development and disease. *Annu Rev Neurosci* 28:127–156.
34. Wang CL, et al. (2007) Activity-dependent development of callosal projections in the somatosensory cortex. *J Neurosci* 27(42):11334–11342.
35. Innocenti GM (1981) Growth and reshaping of axons in the establishment of visual callosal connections. *Science* 212(4496):824–827.
36. Innocenti GM, Frost DO (1979) Effects of visual experience on the maturation of the efferent system to the corpus callosum. *Nature* 280(5719):231–234.
37. Hackett TA, Stepniewska I, Kaas JH (1999) Callosal connections of the parabelt auditory cortex in macaque monkeys. *Eur J Neurosci* 11(3):856–866.
38. Hedin-Pereira C, Lent R, Jhaveri S (1999) Morphogenesis of callosal arbors in the parietal cortex of hamsters. *Cereb Cortex* 9(1):50–64.
39. Lee CC, Schreiner CE, Imaizumi K, Winer JA (2004) Tonotopic and heterotopic projection systems in physiologically defined auditory cortex. *Neuroscience* 128(4): 871–887.
40. Nishikimi M, Oishi K, Tabata H, Torii K, Nakajima K (2011) Segregation and pathfinding of callosal axons through EphA3 signaling. *J Neurosci* 31(45):16251–16260.
41. Lindwall C, Fothergill T, Richards LJ (2007) Commissure formation in the mammalian forebrain. *Curr Opin Neurobiol* 17(1):3–14.
42. Flanagan JG, Vanderhaeghen P (1998) The ephrins and Eph receptors in neural development. *Annu Rev Neurosci* 21:309–345.
43. Serafini T, et al. (1996) Netrin-1 is required for commissural axon guidance in the developing vertebrate nervous system. *Cell* 87(6):1001–1014.
44. Islam SM, et al. (2009) Draxin, a repulsive guidance protein for spinal cord and forebrain commissures. *Science* 323(5912):388–393.
45. Shu T, Richards LJ (2001) Cortical axon guidance by the glial wedge during the development of the corpus callosum. *J Neurosci* 21(8):2749–2758.
46. Shu T, Puche AC, Richards LJ (2003) Development of midline glial populations at the corticoseptal boundary. *J Neurobiol* 57(1):81–94.
47. Keeble TR, et al. (2006) The Wnt receptor Ryk is required for Wnt5a-mediated axon guidance on the contralateral side of the corpus callosum. *J Neurosci* 26(21):5840–5848.
48. Ito A, et al. (2010) Tsukushi is required for anterior commissure formation in mouse brain. *Biochem Biophys Res Commun* 402(4):813–818.
49. Tran TS, Kolodkin AL, Bharadwaj R (2007) Semaphorin regulation of cellular morphology. *Annu Rev Cell Dev Biol* 23(1):263–292.
50. Bagnard D, Lohrum M, Uziel D, Püschel AW, Bolz J (1998) Semaphorins act as attractive and repulsive guidance signals during the development of cortical projections. *Development* 125(24):5043–5053.
51. Takahashi T, et al. (1999) Plexin-neuropilin-1 complexes form functional semaphorin-3A receptors. *Cell* 99(1):59–69.
52. Saito T (2006) In vivo electroporation in the embryonic mouse central nervous system. *Nat Protoc* 1(3):1552–1558.
53. Paxinos G, Halliday G, Watson C, Koutcherov Y, Wang H (2007) *Atlas of the Developing Mouse Brain at E17.5, P0 and P6* (Elsevier, Burlington, MA).
54. Birren SJ, Lo L, Anderson DJ (1993) Sympathetic neuroblasts undergo a developmental switch in trophic dependence. *Development* 119(3):597–610.
55. Chen G, et al. (2008) Semaphorin-3A guides radial migration of cortical neurons during development. *Nat Neurosci* 11(1):36–44.